THE JOURNAL OF PHYSICAL CHEMISTRY C
A JOURNAL OF THE AMERICAN CHEMICAL SOCIETY

pubs.acs.org/JPCC

Article

Formation and Dissociation of Dimethyl Ether Clathrate Hydrate in Interstellar Ice Mimics

Bijesh K. Malla, Gaurav Vishwakarma, Soham Chowdhury, Samir Kumar Nayak, Sharma S. R. K. C. Yamijala, and Thalappil Pradeep*

Cite This: J. Phys. Chem. C 2024, 128, 2463−2470

Read Online

ACCESS | Metrics & More | Article Recommendations | Supporting Information

ABSTRACT: Clathrate hydrates (CHs) are believed to exist within interstellar environments, potentially contributing to the preservation of diverse volatile compounds within icy bodies across the cosmos. In this study, using reflection absorption infrared spectroscopy, we show the formation of dimethyl ether (DME) CH from a vapor-deposited DME−water amorphous ice mixture. Experiments were conducted in an environment mimicking interstellar conditions: ultrahigh vacuum ($P \sim 5 \times 10^{-10}$ mbar) and cryogenic conditions ($T \sim 10$−150 K). Thermal annealing of the amorphous ice mixture to a higher temperature ($T \sim 125$ K) resulted in the formation of CH. Quantum chemical calculations suggested the formation of $5^{12}6^4$ cages of structure II CH. Subsequent investigations into the dissociation of DME CH unveiled its transformation into hexagonal ice, requiring a substantial activation energy of 68.04 kJ mol^{-1}. Additionally, confirmation of the formation and dissociation of CH was supported by temperature-programmed desorption mass spectrometry. These results significantly advance our understanding of the existence of CHs under extreme conditions relevant to an interstellar medium.

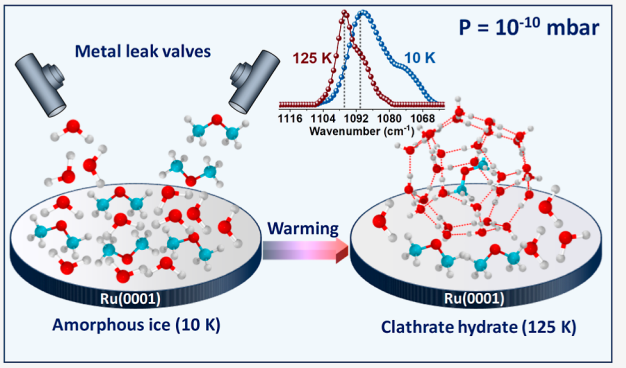

INTRODUCTION

Clathrate hydrates (CHs) are host−guest crystalline compounds having hydrogen-bonded cages of water with different molecules (mostly gases) encaged within.[1−3] While the most common CH structures, known as structure I (sI) and structure II (sII), are cubic and formed with small molecules CH_4, CO_2, C_2H_6, O_2, and N_2 within them, large molecules such as 2-methylbutane and cycloheptane form the hexagonal structure H (sH) CH.[3−6] The formation of this nonstoichiometric crystalline CH is well-known under high-pressure and low-temperature conditions.[7] However, its existence in ultrahigh vacuum (UHV) under cryogenic conditions was established only recently.[8,9] Considering the temperature−pressure conditions, it is now clear that they can occur in outer space in addition to icy environments on earth's sea beds.[10−12] CHs have garnered significant scientific interest due to their potential implications in energy storage,[13] climate change,[10] and astrochemistry.[14,15] Thus, understanding the properties and behavior of CHs is crucial for a wide range of applications.

The formation of CHs in a vacuum at temperatures ranging from 100 to 150 K has been a known phenomenon since the 1990s.[16,17] However, recent advancements have expanded our understanding of CH formation, particularly in the UHV environment at exceptionally low temperatures. These breakthroughs were achieved by thermal annealing of amorphous water matrices in the presence of hydrocarbons like CH_4 (at 30 K)[18] and C_2H_6 (at 60 K)[19] for extended durations, leading to the formation of sI CH. Moreover, it has been observed that the dissociation of the CH of carbonyl compounds such as formaldehyde, acetaldehyde, and acetone can catalyze the formation of hexagonal and cubic crystalline ice structures.[20−22] These findings mark significant progress in our comprehension of CH evolution and hold promise for myriad applications in materials science, cryogenic chemistry, and astrochemistry. Thus, it is imperative to expand our investigative scope to encompass a broader spectrum of molecules studied under a simulated interstellar medium (ISM).

The simplest ether, dimethyl ether (DME), emerges as a molecule of profound significance, showcasing its relevance in the terrestrial environment and ISM.[23−25] It is one of the most abundant complex organic molecules detected in space,[26] and its presence in interstellar clouds and protostellar environments offer valuable insights into the chemistry of the

Received: November 28, 2023
Revised: January 14, 2024
Accepted: January 16, 2024
Published: February 6, 2024

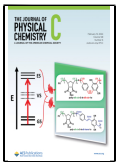

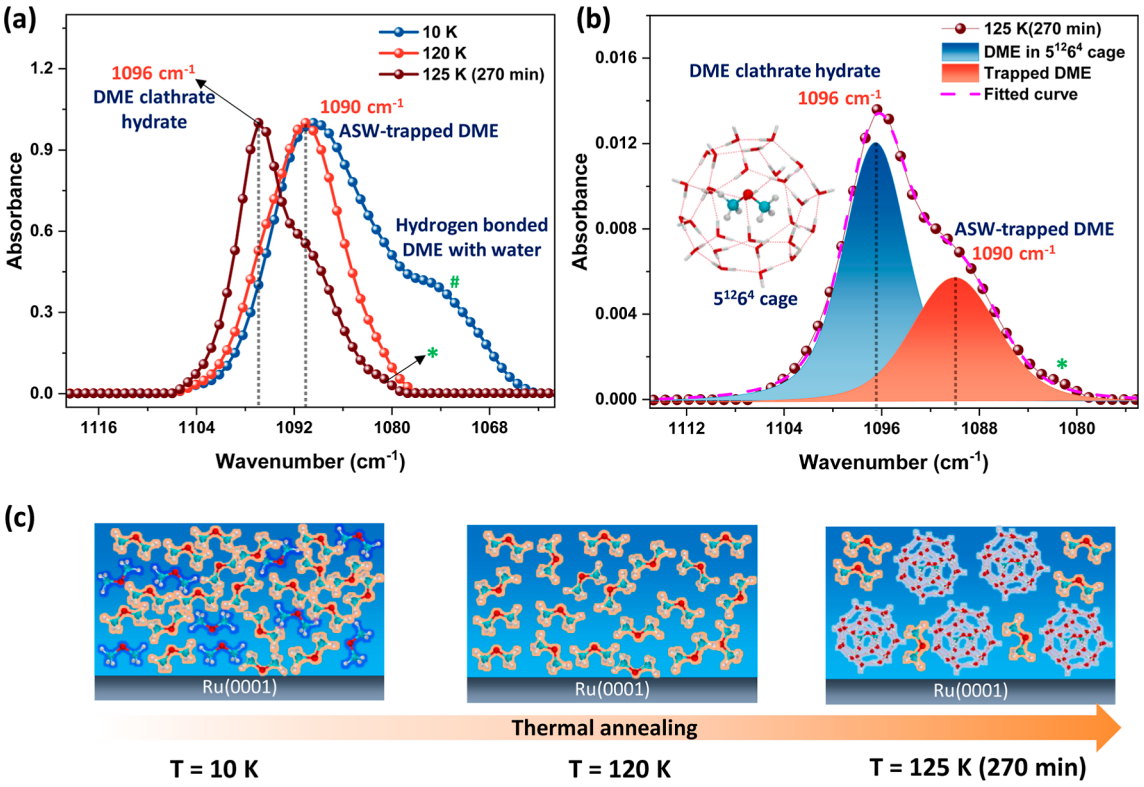

Figure 1. RAIRS study of DME CH. (a) Normalized temperature-dependent RAIR spectra of 300 ML of a DME–H_2O (1:5) ice mixture in the C–O antisymmetric stretching region of DME. (b) IR spectrum after 270 min at 125 K is deconvoluted into two components, shown in blue (peak centered at 1096 cm^{-1}) and red (peak centered at 1090 cm^{-1}) shades. The DFT-optimized structure of DME inside the $5^{12}6^4$ cage is shown in the inset. The peak labeled as * in the spectrum at 125 K and 270 min is attributed to a very tiny amount of dilutes. The ice mixture was codeposited on the Ru(0001) surface at 10 K and annealed to 125 K with a ramping rate of 2 K min^{-1}. (c) Schematic illustration of DME interaction with water at various temperatures. Blue and orange-colored DME molecules represent the strong and weak hydrogen bonding nature of water molecules, respectively, and engaged DME inside $5^{12}6^4$ cages is also shown.

cosmos.[25,27−29] DME is a precursor molecule for forming many organic compounds such as methyl formate, methanol, formaldehyde, methane, and ozone, including those necessary for life.[25] On earth, DME has become a clean-burning alternative fuel and aerosol propellant, contributing to sustainable energy solutions.[30] Thus, DME plays a dual role as both an eco-friendly fuel source on our planet and a crucial molecule in unraveling the mysteries of the ISM.

DME CH is well-studied in high-pressure systems by nuclear magnetic resonance, X-ray diffraction, and Raman spectroscopy.[31−33] Buch et al.[34] showed the formation of sII DME CH by depositing DME vapor on ice nanocrystals. However, no reports of DME CH under UHV and cryogenic conditions exist. In this study, we investigated the formation of sII DME CH using reflection absorption infrared spectroscopy (RAIRS) and temperature-programmed desorption mass spectrometry (TPD-MS). Further, we elucidated the cage selectivity phenomenon by employing quantum chemical calculations. Through controlled thermal annealing, we induced the transformation of an amorphous DME–water ice mixture into the distinct $5^{12}6^4$ cage structure of sII CH. Furthermore, we observed that the dissociation of DME CH leads to the formation of stable hexagonal ice (I_h), requiring a substantial activation energy of 68.04 kJ mol^{-1}. This is the first detailed study investigating the formation and evolution of DME CH under simulated ISM conditions.

EXPERIMENTAL SECTION

All experiments were conducted inside a UHV chamber, maintaining a base pressure of ~5 × 10^{-10} mbar. The apparatus is described in detail elsewhere.[35] Briefly, this vacuum chamber is equipped with several analytical techniques, including RAIRS, TPD-MS, secondary ion mass spectrometry, low energy ion scattering mass spectrometry, and a VUV lamp. The base pressure of the vacuum chamber is maintained by several turbomolecular pumps, further backed by several oil-free diaphragm pumps. A single crystal Ru(0001) surface 1.5 cm in diameter and 1 mm in thickness was used for our experiments to grow thin ice films. This substrate was securely mounted on a copper holder and positioned at the tip of a closed-cycle helium cryostat. The substrate is also equipped with a 25 Ω resistive heater, allowing precise temperature control in the range of 8 to 1000 K. Temperature measurement was achieved using a K-type thermocouple and a platinum sensor, providing a temperature accuracy of 0.5 K. Before each experiment, Ru(0001) was heated to 400 K repeatedly to ensure cleanliness. It is worth noting that the surface has no effect in this study due to multilayer deposition.

Millipore water (H_2O of 18.2 MΩ resistivity) was taken in a vacuum-sealed test tube (with a glass-to-metal seal) and was further purified by several freeze–pump–thaw cycles. DME (99.9%, Sigma-Aldrich) was used without further purification. DME and water were connected to the UHV chamber through separate sample inlet lines. Precise control over the deposition of these two samples was achieved by utilizing all-metal leak

https://doi.org/10.1021/acs.jpcc.3c07792
J. Phys. Chem. C 2024, 128, 2463−2470

valves. For quantification purposes, we considered that 1.33×10^{-6} mbar exposure for a second equated to 1 monolayer (ML), which in turn was estimated to contain approximately 1.1×10^{15} molecules cm^{-2}, assuming a sticking coefficient of unity.[36] To deposit 300 ML of ice consisting of a 1:1 ratio of DME and water mixture, the chamber was backfilled to a total pressure of 5×10^{-7} mbar for 10 min, with DME reaching 2.5×10^{-7} mbar and water pressure also maintained at 2.5×10^{-7} mbar. Different ratios of DME and H_2O/D_2O (1:5, 1:10, and 1:20) were prepared at 10 K by keeping the total pressure constant and varying the inlet pressure of DME and water accordingly. Throughout the vapor deposition process, mass spectra were continuously recorded to verify both the purity and the ratio of the deposited molecules.

The formation of DME CH was investigated by using both RAIR spectroscopy and TPD mass spectrometry. RAIR spectra were obtained in the 4000−550 cm^{-1} range with a spectral resolution of 2 cm^{-1} utilizing a Bruker Vertex 70 FT-IR spectrometer equipped with a liquid nitrogen-cooled mercury cadmium telluride detector. The IR beam path outside the UHV chamber was continuously purged with dry nitrogen to avoid absorption by atmospheric gases. For the TPD-MS experiments, we employed a quadrupole mass spectrometer supplied by Extrel.

COMPUTATIONAL DETAILS

All of the electronic structure calculations were conducted using the Gaussian 09 software package. First, the ground-state geometries of the DME and the CH cages (namely, the 5^{12}, $5^{12}6^2$, and $5^{12}6^4$ cages) were optimized using the density functional theory at the B3LYP/6-311++g(d,p) level of theory.[19] Next, the optimized DME molecule was placed inside the optimized CH cages, and the geometries were reoptimized at the same level of theory. Additionally, we conducted frequency calculations to verify that these geometries are at the minimum of the potential energy surface, and these calculations always yielded nonimaginary frequencies, proving the ground-state nature of these geometries.

RESULTS AND DISCUSSION

The DME CH was created by slow annealing the vapor-deposited amorphous DME−water ice mixture from 10 to 125 K. Three hundred monolayers of DME and water (1:5) ice mixture were codeposited on the Ru(0001) substrate at 10 K, then slowly annealed to 125 K with a ramping rate of 2 K min^{-1} and waited there for 270 min. Figure 1a shows the normalized RAIR spectra of DME at 10, 120, and 125 K (after waiting for 270 min) in the C−O antisymmetric stretching region. The RAIR spectrum at 10 K shows a peak at 1090 cm^{-1} and is accompanied by a broad IR band centered around 1075 cm^{-1}, which is 8 and 23 cm^{-1} red-shifted from the pure amorphous DME peak at 10 K, respectively (the RAIR spectra of pure amorphous DME are shown in Figure S1a). The peaks at 1090 and 1075 cm^{-1} can be attributed to the hydrogen bonding (weak and strong) interaction of DME with water molecules.[37] The broad shoulder near 1075 cm^{-1} disappeared with a reduction in the peak intensity at 1090 cm^{-1} when the ice mixture was annealed to 120 K (Figure S2), suggesting the weakening of DME−water hydrogen bonding at higher temperatures and fractional desorption of DME from the ice matrix. Understanding the weakening of hydrogen bonding is facilitated by analyzing the temperature-dependent RAIR spectra of DME−water (1:1) presented in Figure S3a. This analysis reveals a notable reduction in the intensity of the broad peak (#) and a concurrent increase in the intensity at the 1090 cm^{-1} peak. These changes are observed before the desorption temperature of pure DME (90 K), as illustrated in Figure S6. Further annealing the mixture from 120 to 125 K gives rise to a new peak at 1096 cm^{-1} (Figure S2a), attributed to the DME engaged in CH cages.[37] Upon isothermal annealing at 125 K, a gradual decrease in the peak intensity of 1090 cm^{-1} was observed for 180 min; afterward, no further changes until 270 min were observed. This decrease represents the desorption of trapped DME from amorphous solid water (ASW) up to a specific point in time; beyond this point, prolonged waiting does not result in further desorption. By deconvoluting the spectrum at 125 K after 270 min (shown in Figure 1b), we found that 25.3% of the total DME was exclusively encaged in the CH structure, while 15.5% of the total DME was observed to be trapped within the ASW matrix. Additionally, in the C−O symmetric stretching region, a new peak was observed at 928 cm^{-1} upon the formation of CH, which was absent at 10 K (shown in Figure S2b). To investigate the influence of the DME−water ratio on the CH formation fraction, we conducted four temperature-dependent RAIR experiments using different mixtures (1:1, 1:5, 1:10, and 1:20) of DME and water. These various ice mixtures were deposited at 10 K and subsequently subjected to direct annealing at 130 K, with the resulting fraction of DME encaged in CH being calculated and presented in Table S1. Remarkably, the highest observed fraction was 16% for the 1:5 ratio, while the lowest was 6.5% for the 1:20 ratio. It is important to note that the temperature, ratio of host and guest molecules, and annealing time influence CH formation in UHV conditions.[18,19]

The reported crystal structure of DME CH suggests the formation of sII and a tetragonal structure from an aqueous solution of DME at a temperature of −40 °C.[31] However, under low-temperature conditions, only sII hydrate was obtained upon vapor deposition of DME on ice nanocrystals.[34] DME has a molecular size of 4.1 Å,[38] whereas the sII small and large cages have an average cavity radius of 3.91 and 4.73 Å, respectively.[6] This suggests that DME prefers to form large cages rather than small ones. In the current study, we observed 6 and 12 cm^{-1} blue-shifted peaks in C−O antisymmetric and symmetric stretching regions, respectively, after annealing to 125 K. This same shift was also observed when we performed a temperature-dependent RAIR study, taking H_2O−DME and D_2O−DME ice mixtures at a higher temperature (>130 K) (shown in Figures S3 and S4). Also, sequentially deposited DME and a water−ice mixture showed CH formation above 130 K (Figure S5). A new single peak arises in C−O asymmetric and symmetric stretching, suggesting the formation of single types of cages attributed to the sII large cage. Buch et al.[34] showed the formation of DME and H_2S CH where H_2S occupied the small cage, most parts of DME occupied the large cage, and other fractions stayed as absorbed molecules in the system. The resulting RAIR spectrum we obtained after 270 min at 125 K (Figure 1a) matches the infrared spectrum shown by Buch et al. in their study.[34] So, the new peak at 1096 cm^{-1} can be attributed to the large cage ($5^{12}6^4$) of sII CH, and the peak at 1090 cm^{-1} indicates the presence of trapped DME within the ASW matrix.

To further strengthen our claim on the formation of a large cage ($5^{12}6^4$) of sII, we conducted quantum chemical

https://doi.org/10.1021/acs.jpcc.3c07792
J. Phys. Chem. C 2024, 128, 2463−2470

calculations of DME in various CH cages and computed the infrared spectra of such clathrates. Our simulations yielded significant shifts in the vibrational frequencies after the inclusion of guest molecules into the CH cages, elucidating the diverse structural conformations of CH. Figure 2 shows the

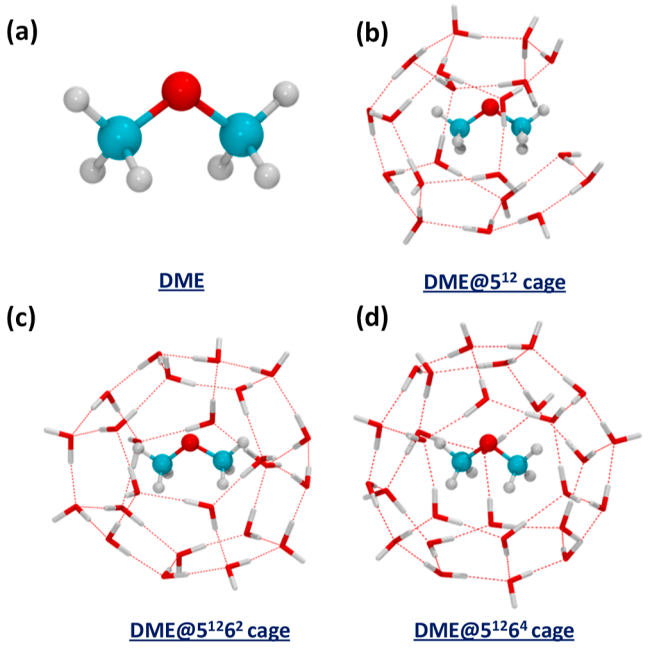

Figure 2. DFT-optimized structures of DME and DME trapped within different CH cages, such as (a) DME, (b) 5^{12} cage, (c) $5^{12}6^2$ cage, and (d) $5^{12}6^4$ cage. Color code used: cyan, C; red, O; and gray, H.

DFT-optimized structures of DME and DME encaged in 5^{12}, $5^{12}6^2$, and $5^{12}6^4$ cages. It was observed that DME in $5^{12}6^2$ and $5^{12}6^4$ is stable, whereas in the 5^{12} cage, it is unstable, leading to the cage breaking (Figure 2b). The vibrational frequency of free DME and DME encaged in $5^{12}6^2$ and $5^{12}6^4$ cages in the C−O antisymmetric stretching region is presented in Table S2. It was found that in the case of the $5^{12}6^2$ cage, DME shows a positive shift of 3.05 cm^{-1}, and in the case of the $5^{12}6^4$, it shows a negative shift of 3.21 cm^{-1}. It is important to note that DME has a molecular size of 4.1 Å, with the average cavity radius of $5^{12}6^2$ and $5^{12}6^4$ being 4.33 and 4.73 Å, respectively.[6] In the case of the $5^{12}6^2$ cage, the larger methyl groups of DME hinder the oxygen atom from approaching the clathrate cage walls,[38] resulting in increased steric hindrance and, consequently, a blue shift in frequency. Conversely, the $5^{12}6^4$ cage, with its larger cavity radius, allows for closer proximity between the oxygen atom and the hydrogen atoms of the cage walls, promoting hydrogen bonding and leading to a red shift in the frequency. Experimentally, we observed that pure amorphous DME shows a peak at 1098 cm^{-1}, whereas the DME CH shows a peak at 1096 cm^{-1}, indicating a 2 cm^{-1} redshift. Theoretical calculations reveal that pure DME has a peak at 1090.93 cm^{-1}, whereas DME encaged in the $5^{12}6^4$ cage exhibits a peak at 1187.72 cm^{-1}, corresponding to a 3.2 cm^{-1} redshift. Notably, the experimental shift closely matches the theoretical shift in the $5^{12}6^4$ cage (the large cage of sII). From all of these results, we infer that DME forms the $5^{12}6^4$ cage of sII CH under UHV and cryogenic conditions.

The observation of outgassing patterns within the cometary environment has significantly enhanced our comprehension of various types of ice, such as crystalline ice and CH.[11] Here, with the help of TPD-MS, we showed that the DME molecules encaged in the CH cage and a fraction of molecules trapped in the ASW matrix desorb in a molecular volcano (MV) event during the phase transition to crystalline ice.[39,40] To form DME CH, we vapor-deposited 300 ML of a DME−water (1:5) ice mixture at 10 K, annealed the system to 130 K, and then waited for 2 h to desorb the maximum residual molecules not trapped inside the cages. Subsequently, we cooled the system back to 10 K, annealed the DME CH to 200 K with a ramping rate of 10 K min^{-1}, and collected the mass spectra to measure

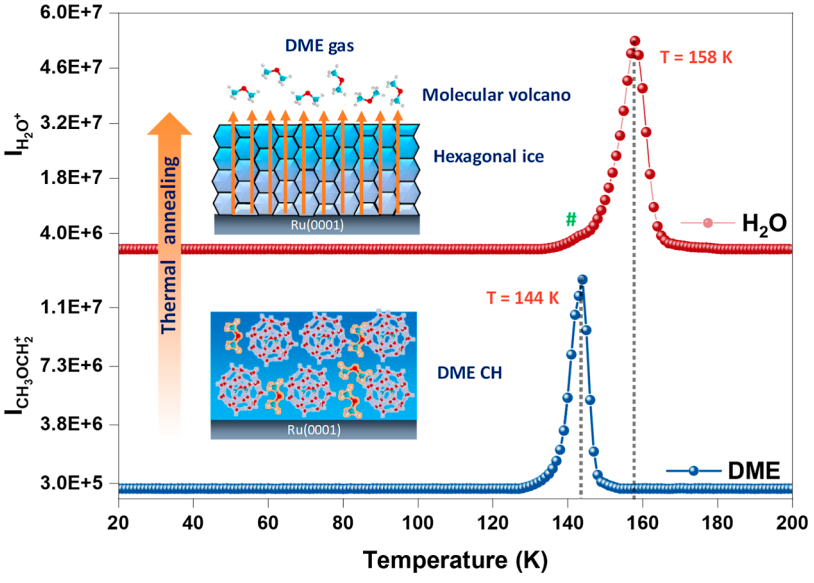

Figure 3. TPD-MS study of DME CH. TPD mass spectra of 300 ML of a DME−H_2O (1:5) ice mixture after hydrate formation. The red spectrum represents the H_2O desorption, and the blue spectrum represents the DME desorption. Mass spectra are plotted between the intensity of H_2O^+ (m/z = 18) and $CH_3OCH_2^+$ (m/z = 45) with respect to temperature. The peak labeled (#) is attributed to a phase transition from CH to I_h. A schematic illustration of the MV event or transition from DME CH to I_h is shown inside the plot.

https://doi.org/10.1021/acs.jpcc.3c07792
J. Phys. Chem. C 2024, 128, 2463−2470

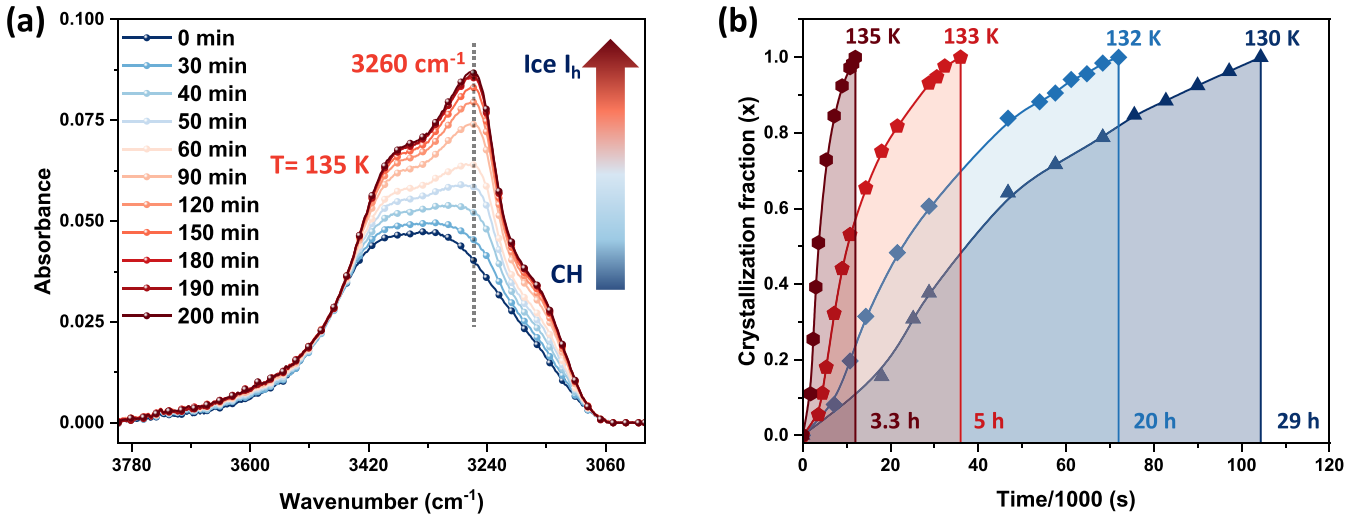

Figure 4. (a) Time-dependent RAIR spectra of 300 ML of the DME−H_2O (1:5) ice mixture at 135 K in the O−H stretching region. The vertical cut at 3260 cm^{-1} was utilized to determine the crystallization fraction. (b) Crystallization fraction vs time for 300 ML of the DME−H_2O (1:5) ice mixture at 130, 132, 133, and 135 K. The vertical cut for the crystallization fraction at different temperatures shows the crystallization half-time.

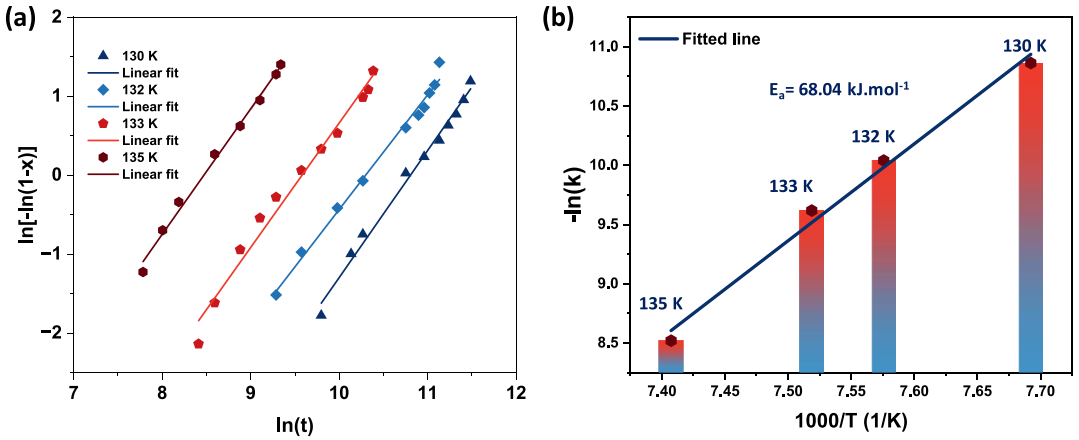

Figure 5. (a) Plot of the linearized form of the Avrami equation for ASW crystallization. Plots of $\ln(-\ln[1-x])$ versus $\ln(t)$ at different temperatures of 130, 132, 133, and 135 K were evaluated using the O−H stretching bands. The obtained data points were fitted using the Avrami equation. (b) Arrhenius plot of $-\ln k$ versus $(1/T)$, achieved from the analysis of the slope and intercept of the linearly fitted lines of the plot (a) for different temperatures. The activation energy (E_a) of ice crystallization was calculated from the slope of the linearly fitted straight line of plot (b).

the intensities at m/z = 18 (water) and m/z = 45 (DME). In Figure 3, the blue and red spectra represent the mass spectra for DME and water, respectively. The peak at 144 K (in the blue spectrum) is attributed to the MV peak. When the water molecules participating in CH cages turn to I_h along with ASW, all of the cages are broken, resulting in the desorption of molecules at a time showing a sharp MV peak. The phase transition (CH to I_h) peak in the red spectrum is shown by #. The peak at 158 K in the red spectrum represents the sublimation of the water matrix. While pure DME endures in the solid phase up to 93 K (Figure S6), DME in CH form is stable in the solid phase until 144 K in UHV conditions. This suggests the possibility of the presence of DME in the hot core regions of the ISM. A parallel experiment utilizing deuterated water yielded similar results, with the MV peak observed at 147 K for DME and a water desorption peak at 161 K due to the bulkier mass and reduced mobility of deuterated water molecules (shown in Figure S7).

The study of crystallization kinetics, specifically focusing on the transition from CH to I_h, holds significant relevance in various scientific disciplines, including CH chemistry, physical chemistry, astrochemistry, and planetary science.[41−44] We conducted isothermal time-dependent RAIRS experiments utilizing a 300 ML DME−water (1:5) film within the temperature range 130−135 K to assess the kinetic parameters of this phase transition. Figure 4a shows the time-dependent data in the O−H stretching region. At 0 min, the spectrum represents the water molecules that participated in the CH phase and the remaining ASW. The 200 min spectrum represents the I_h crystalline feature, comparable to the previous literature.[45−48] It is well-known that pure amorphous ice converts to I_h at elevated temperatures in UHV.[47] We have created I_h from pure amorphous water at 140 K and compared it with our results (Figure S8). The crystallization fraction at different temperatures versus time is shown in Figure 4b (calculated from the infrared spectra shown in Figure S9). The absorbance intensity at 3260 cm^{-1} was used to evaluate the crystallization fraction, $x(t)$ using eq 1.

https://doi.org/10.1021/acs.jpcc.3c07792
J. Phys. Chem. C 2024, 128, 2463−2470

$$x(t) = \frac{\Delta A(1)}{\Delta A(2)} \quad (1)$$

$\Delta A(1)$ represents the difference between absorbance at a specific time t and one at time 0, and $\Delta A(2)$ is the corresponding value for the difference between the absorbance at time 0 and a completely crystallized film. Thermodynamics of the dissociation of CH and its impact on the crystallization of water ice can be understood from the crystallization fraction. The observed crystallization times indicate a significant difference, with 29 h required at 130 K and only 3.3 h at 135 K. This strongly suggests that higher temperatures facilitate a more rapid dissociation of DME CH, enhancing the crystallization kinetics. To underscore this point further, we conducted a comparative analysis of the crystallization fraction for DME CH and pure water at 130 K, as depicted in Figure S10. Notably, in the case of pure water at 135 K, a considerably extended period of 12 h was necessary for crystallization to occur. This further supports the correlation between the elevated temperature, increased DME CH dissociation, and accelerated crystallization kinetics.

Kinetics parameters and activation energy for the CH to I_h transition were evaluated using the Avrami equation.[49,50]

$$x(t) = 1 - \exp(-k \cdot t)^n \quad (2)$$

where k is the rate constant, t is the time, and n is a parameter related to the crystallization mechanism.[50] The variable "n" can take values within the range of 1 to 4, and these values are used to predict the nature of the crystallization process.[51,52] eq 2 can be rearranged in a linear form.

$$\ln(-\ln[1 - x(t)]) = n \ln(t) + n \ln k \quad (3)$$

Figure 5a shows plots of $\ln(-\ln[1 - x(t)])$ versus $\ln(t)$ at different temperatures. The values of n and k at various temperatures were calculated using the slope and intercept of linearly fitted lines and are shown in Table 1. The value

Table 1. Kinetics Parameters Estimated Using the Avrami Equation at Various Temperatures

temperature (K)	130	132	133	135
n	1.60	1.45	1.57	1.58
rate constant (k)	1.9×10^{-5}	4.3×10^{-5}	6.65×10^{-5}	1.9×10^{-4}

obtained for n is found between 1.4 and 1.6, indicating that the nucleation started from CH and amorphous ice interfaces and grew in a polyhedral manner in the side ice matrix.[21,52,53] The slope of the linearly fitted line of the Arrhenius plot (Figure 5b) was used to determine the activation energy (E_a) of ice crystallization. It was found to be 68.04 kJ mol^{-1} for the transition from CH to I_h. Our previous studies reported that the activation energy for the desorption-induced ASW to I_h transition is ~52−58 kJ mol^{-1},[20,45,46] less than the value from the current study. This suggests that the higher thermodynamic stability of DME CH leads to its slow transformation to I_h.

CONCLUSIONS

Here, we show the formation of sII DME CH in DME−H_2O interstellar ice mimics. A vapor-deposited amorphous DME and water ice mixture was created at 10 K in UHV; its further annealing to 125 K resulted in a new IR peak at 1096 cm^{-1}, indicating the formation of DME CH. Quantum chemical calculations provided compelling evidence for the creation of the large cage structure ($5^{12}6^4$) of sII. Additionally, TPD-MS revealed the phenomenon of DME molecules desorbing in a MV event during the transition from CH to crystalline ice. The RAIR study showed that CH resulted in the formation of I_h upon dissociation. The kinetics of crystallization were systematically analyzed using the Avrami equation, revealing a kinetic energy requirement of 68.04 kJ mol^{-1} for the dissociation and subsequent formation of I_h. These findings provide a comprehensive mechanistic insight into the formation and dissociation of DME CH within interstellar environments, advancing our understanding of complex processes occurring within such celestial settings.

ASSOCIATED CONTENT

Supporting Information

The Supporting Information is available free of charge at https://pubs.acs.org/doi/10.1021/acs.jpcc.3c07792.

Temperature- and time-dependent RAIR, TPD-MS spectra of pure DME, and DME−water ice mixtures (PDF)

AUTHOR INFORMATION

Corresponding Author

Thalappil Pradeep − *Department of Science and Technology Unit of Nanoscience (DST UNS) and Thematic Unit of Excellence (TUE), Department of Chemistry, Indian Institute of Technology Madras, Chennai 600036, India; Centre of Excellence on Molecular Materials and Functions, Indian Institute of Technology Madras, Chennai 600036, India; International Centre for Clean Water, Chennai 600113, India;* orcid.org/0000-0003-3174-534X; Email: pradeep@iitm.ac.in

Authors

Bijesh K. Malla − *Department of Science and Technology Unit of Nanoscience (DST UNS) and Thematic Unit of Excellence (TUE), Department of Chemistry, Indian Institute of Technology Madras, Chennai 600036, India*

Gaurav Vishwakarma − *Department of Science and Technology Unit of Nanoscience (DST UNS) and Thematic Unit of Excellence (TUE), Department of Chemistry, Indian Institute of Technology Madras, Chennai 600036, India*

Soham Chowdhury − *Department of Science and Technology Unit of Nanoscience (DST UNS) and Thematic Unit of Excellence (TUE), Department of Chemistry, Indian Institute of Technology Madras, Chennai 600036, India*

Samir Kumar Nayak − *Department of Chemistry, Indian Institute of Technology Madras, Chennai 600036, India*

Sharma S. R. K. C. Yamijala − *Department of Chemistry, Centre for Atomistic Modelling and Materials Design, Centre for Quantum Information, Communication, and Computing, and Centre of Excellence on Molecular Materials and Functions, Indian Institute of Technology Madras, Chennai 600036, India;* orcid.org/0000-0003-1773-9226

Complete contact information is available at: https://pubs.acs.org/10.1021/acs.jpcc.3c07792

https://doi.org/10.1021/acs.jpcc.3c07792
J. Phys. Chem. C 2024, 128, 2463−2470

Author Contributions

B.K.M. and T.P. designed the experiments, B.K.M., G.V., and S.C. performed the experiments and analyzed the results. T.P. proposed the project and supervised the progress. S.K.N. and S.S.R.K.C.Y. performed the quantum chemical calculations. The manuscript was written with the contributions of all authors.

Notes

The authors declare no competing financial interest.

■ ACKNOWLEDGMENTS

We acknowledge the Science and Engineering Research Board (SERB), Department of Science and Technology (DST), and the Government of India for their research funding. T.P. acknowledges funding from the Centre of Excellence on Molecular Materials and Functions under the Institution of Eminence scheme of IIT Madras. S.S.R.K.C.Y. acknowledges the financial support of IIT Madras through its new faculty support grants NFSG (IP2021/0972CY/NFSC008973), NFIG (RF2021/0577CY/NFIG 008973), and DST-SERB (SRG/2021/001455). B.K.M. thanks the Council of Scientific and Industrial Research (CSIR) for his research fellowship. G.V. and S.C. thank IITM for their research fellowship. S.K.N. thanks the Prime Minister's Research Fellowship (PMRF) for his research fellowship.

■ REFERENCES

(1) Davy, H. VIII. On a Combination of Oxymuriatic Gas and Oxygene Gas. *Philos. Trans. R. Soc. London* **1811**, *101*, 155−162.
(2) Sloan, E. D. Fundamental Principles and Applications of Natural Gas Hydrates. *Nature* **2003**, *426*, 353−359.
(3) Devlin, J. P. Structure, Spectra, and Mobility of Low-pressure Ices: Ice I, Amorphous Solid Water, and Clathrate Hydrates at T < 150 K. *J. Geophys. Res.: Planets* **2001**, *106* (E12), 33333−33349.
(4) Ratcliffe, C. I. The Development of Clathrate Hydrate Science. *Energy Fuels* **2022**, *36* (18), 10412−10429.
(5) Truong-Lam, H. S.; Seo, S.; Kim, S.; Seo, Y.; Lee, J. D.; Lee, J. D. In Situ Raman Study of the Formation and Dissociation Kinetics of Methane and Methane/Propane Hydrates. *Energy Fuels* **2020**, *34* (5), 6288−6297.
(6) Sloan, E. D.; Koh, C. A.; Koh, C. A. *Clathrate Hydrates of Natural Gases*; CRC Press, 2007.
(7) Khurana, M.; Yin, Z.; Linga, P. A Review of Clathrate Hydrate Nucleation. *ACS Sustain. Chem. Eng.* **2017**, *5* (12), 11176−11203.
(8) Ghosh, J.; Vishwakarma, G.; Kumar, R.; Pradeep, T. Formation and Transformation of Clathrate Hydrates under Interstellar Conditions. *Acc. Chem. Res.* **2023**, *56*, 2241−2252.
(9) Vishwakarma, G.; Malla, B. K.; Reddy, K. S. S. V. P.; Ghosh, J.; Chowdhury, S.; Yamijala, S. S. R. K. C.; Reddy, S. K.; Kumar, R.; Pradeep, T. Induced Migration of CO2 from Hydrate Cages to Amorphous Solid Water under Ultrahigh Vacuum and Cryogenic Conditions. *J. Phys. Chem. Lett.* **2023**, *14*, 2823−2829.
(10) Hester, K. C.; Brewer, P. G. Clathrate Hydrates in Nature. *Ann. Rev. Mar. Sci.* **2009**, *1*, 303−327.
(11) Luspay-Kuti, A.; Mousis, O.; Hässig, M.; Fuselier, S. A.; Lunine, J. I.; Marty, B.; Mandt, K. E.; Wurz, P.; Rubin, M. The Presence of Clathrates in Comet 67P/Churyumov-Gerasimenko. *Sci. Adv.* **2016**, *2* (4), No. e1501781.
(12) Mousis, O.; Schmitt, B. Sequestration of Ethane in the Cryovolcanic Subsurface of Titan. *Astrophys. J.* **2008**, *677* (1), L67−L70.
(13) Yin, Z.; Zheng, J.; Kim, H.; Seo, Y.; Linga, P. Hydrates for Cold Energy Storage and Transport: A Review. *Adv. Appl. Energy* **2021**, *2*, 100022.
(14) Devlin, J. P. Structure, Spectra, and Mobility of Low-pressure Ices: Ice I, Amorphous Solid Water, and Clathrate Hydrates at T < 150 K. *J. Geophys. Res.: Planets* **2001**, *106* (E12), 33333−33349.
(15) Thomas, C.; Mousis, O.; Picaud, S.; Ballenegger, V. Variability of the Methane Trapping in Martian Subsurface Clathrate Hydrates. *Planet. Space Sci.* **2009**, *57* (1), 42−47.
(16) Blake, D.; Allamandola, L.; Sandford, S.; Hudgins, D.; Freund, F. Clathrate Hydrate Formation in Amorphous Cometary Ice Analogs in Vacuo. *Science* **1991**, *254* (5031), 548−551.
(17) Fleyfel, F.; Devlin, J. P. FT-IR Spectra of 90 K Films of Simple, Mixed, and Double Clathrate Hydrates of Trimethylene Oxide, Methyl Chloride, Carbon Dioxide, Tetrahydrofuran, and Ethylene Oxide Containing Decoupled Water-D2. *J. Phys. Chem.* **1988**, *92* (3), 631−635.
(18) Ghosh, J.; Methikkalam, R. R. J.; Bhuin, R. G.; Ragupathy, G.; Choudhary, N.; Kumar, R.; Pradeep, T. Clathrate Hydrates in Interstellar Environment. *Proc. Natl. Acad. Sci. U.S.A.* **2019**, *116* (5), 1526−1531.
(19) Malla, B. K.; Vishwakarma, G.; Chowdhury, S.; Selvarajan, P.; Pradeep, T. Formation of Ethane Clathrate Hydrate in Ultrahigh Vacuum by Thermal Annealing. *J. Phys. Chem. C* **2022**, *126* (42), 17983−17989.
(20) Ghosh, J.; Vishwakarma, G.; Das, S.; Pradeep, T. Facile Crystallization of Ice Ihvia Formaldehyde Hydrate in Ultrahigh Vacuum under Cryogenic Conditions. *J. Phys. Chem. C* **2021**, *125* (8), 4532−4539.
(21) Vishwakarma, G.; Malla, B. K.; Chowdhury, S.; Khandare, S. P.; Pradeep, T. Existence of Acetaldehyde Clathrate Hydrate and Its Dissociation Leading to Cubic Ice under Ultrahigh Vacuum and Cryogenic Conditions. *J. Phys. Chem. Lett.* **2023**, *14*, 5328−5334.
(22) Ghosh, J.; Bhuin, R. G.; Vishwakarma, G.; Pradeep, T. Formation of Cubic Ice via Clathrate Hydrate, Prepared in Ultrahigh Vacuum under Cryogenic Conditions. *J. Phys. Chem. Lett.* **2020**, *11* (1), 26−32.
(23) Semelsberger, T. A.; Borup, R. L.; Greene, H. L. Dimethyl Ether (DME) as an Alternative Fuel. *J. Power Sources* **2006**, *156* (2), 497−511.
(24) Terwisscha Van Scheltinga, J.; Ligterink, N. F. W.; Boogert, A. C. A.; Van Dishoeck, E. F.; Linnartz, H. Infrared Spectra of Complex Organic Molecules in Astronomically Relevant Ice Matrices - I. Acetaldehyde, Ethanol, and Dimethyl Ether. *Astron. Astrophys.* **2018**, *611*, A35.
(25) Peeters, Z.; Rodgers, S. D.; Charnley, S. B.; Schriver-Mazzuoli, L.; Schriver, A.; Keane, J. V.; Ehrenfreund, P. Astrochemistry of dimethyl ether. *Astron. Astrophys.* **2006**, *445*, 197−204.
(26) Snyder, L. E.; Buhl, D.; Schwartz, P. R.; Clark, F. O.; Johnson, D. R.; Lovas, F. J.; Giguere, P. T. Radio Detection of Interstellar Dimethyl Ether. *Astrophys. J.* **1974**, *191*, L79.
(27) Modica, P.; Palumbo, M. E. Formation of Methyl Formate after Cosmic Ion Irradiation of Icy Grain Mantles. *Astron. Astrophys.* **2010**, *519* (2), A22.
(28) Cernuto, A.; Tosi, P.; Martini, L. M.; Pirani, F.; Ascenzi, D. Experimental Investigation of the Reaction of Helium Ions with Dimethyl Ether: Stereodynamics of the Dissociative Charge Exchange Process. *Phys. Chem. Chem. Phys.* **2017**, *19* (30), 19554−19565.
(29) Skouteris, D.; Balucani, N.; Ceccarelli, C.; Faginas Lago, N.; Codella, C.; Falcinelli, S.; Rosi, M. Interstellar Dimethyl Ether Gas-Phase Formation: A Quantum Chemistry and Kinetics Study. *Mon. Not. R. Astron. Soc.* **2019**, *482* (3), 3567−3575.
(30) Matzen, M.; Demirel, Y. Methanol and Dimethyl Ether from Renewable Hydrogen and Carbon Dioxide: Alternative Fuels Production and Life-Cycle Assessment. *J. Clean. Prod.* **2016**, *139*, 1068−1077.
(31) Gough, S. R.; Garg, S. K.; Ripmeester, J. A.; Davidson, D. W. Dielectric Relaxation and Nuclear Magnetic Resonance Studies of Two Clathrate Hydrates of Dimethyl Ether. *J. Phys. Chem.* **1977**, *81* (23), 2158−2163.

https://doi.org/10.1021/acs.jpcc.3c07792
J. Phys. Chem. C 2024, 128, 2463−2470

(32) Huang, P.; Liu, X.; Wada, Y.; Katoh, K.; Arai, M.; Tamura, M. Decomposition and Raman Spectrum of Dimethyl Ether Hydrate. *Fuel* **2013**, *105*, 364−367.
(33) Udachin, K. A.; Ratcliffe, C. I.; Ripmeester, J. A. A Dense and Efficient Clathrate Hydrate Structure with Unusual Cages. *Angew. Chem., Int. Ed.* **2001**, *40* (7), 1303−1305.
(34) Buch, V.; Devlin, J. P.; Monreal, I. A.; Jagoda-Cwiklik, B.; Uras-Aytemiz, N.; Cwiklik, L. Clathrate Hydrates with Hydrogen-Bonding Guests. *Phys. Chem. Chem. Phys.* **2009**, *11* (44), 10245−10265.
(35) Bag, S.; Bhuin, R. G.; Methikkalam, R. R. J.; Pradeep, T.; Kephart, L.; Walker, J.; Kuchta, K.; Martin, D.; Wei, J. Development of Ultralow Energy (1−10 EV) Ion Scattering Spectrometry Coupled with Reflection Absorption Infrared Spectroscopy and Temperature Programmed Desorption for the Investigation of Molecular Solids. *Rev. Sci. Instrum.* **2014**, *85* (1), 014103.
(36) Moon, E. S.; Kang, H.; Oba, Y.; Watanabe, N.; Kouchi, A. Direct Evidence for Ammonium Ion Formation in Ice through Ultraviolet-Induced Acid-Base Reaction of NH_3 With H_3O^+. *Astrophys. J.* **2010**, *713* (2), 906−911.
(37) Schriver-Mazzuoli, L.; Coanga, J. M.; Schriver, A.; Ehrenfreund, P. Infrared Spectra of $(CH_3)_2O$ and $(CH_3)_2O$ + H_2O at Low Temperature. *Vib. Spectrosc.* **2002**, *30* (2), 245−257.
(38) Kulig, W.; Kubisiak, P.; Cwiklik, L. Steric and Electronic Effects in the Host-Guest Hydrogen Bonding in Clathrate Hydrates. *J. Phys. Chem. A* **2011**, *115* (23), 6149−6154.
(39) May, R. A.; Smith, R. S.; Kay, B. D. The Release of Trapped Gases from Amorphous Solid Water Films. I. "Top-down" Crystallization-Induced Crack Propagation Probed Using the Molecular Volcano. *J. Chem. Phys.* **2013**, *138*, 104501.
(40) Collings, M. P.; Anderson, M. A.; Chen, R.; Dever, J. W.; Viti, S.; Williams, D. A.; McCoustra, M. R. S. A Laboratory Survey of the Thermal Desorption of Astrophysically Relevant Molecules. *Mon. Not. R. Astron. Soc.* **2004**, *354*, 1133−1140.
(41) Cao, H. S. Formation and Crystallization of Low-Density Amorphous Ice. *J. Phys. D Appl. Phys.* **2021**, *54* (20), 203002.
(42) Takeya, S.; Fujihisa, H.; Alavi, S.; Ohmura, R. Thermally Induced Phase Transition of Cubic Structure II Hydrate: Crystal Structures of Tetrahydropyran-CO2 Binary Hydrate. *J. Phys. Chem. Lett.* **2023**, *14* (7), 1885−1891.
(43) Minissale, M.; Aikawa, Y.; Bergin, E.; Bertin, M.; Brown, W. A.; Cazaux, S.; Charnley, S. B.; Coutens, A.; Cuppen, H. M.; Guzman, V.; et al. Thermal Desorption of Interstellar Ices: A Review on the Controlling Parameters and Their Implications from Snowlines to Chemical Complexity. *ACS Earth Space Chem.* **2022**, *6* (3), 597−630.
(44) Bartels-Rausch, T.; Bergeron, V.; Cartwright, J. H. E.; Escribano, R.; Finney, J. L.; Grothe, H.; Gutiérrez, P. J.; Haapala, J.; Kuhs, W. F.; Pettersson, J. B. C.; et al. Ice Structures, Patterns, and Processes: A View across the Icefields. *Rev. Mod. Phys.* **2012**, *84* (2), 885−944.
(45) Vishwakarma, G.; Malla, B. K.; Methikkalam, R. R. J.; Pradeep, T. Rapid Crystallization of Amorphous Solid Water by Porosity Induction. *Phys. Chem. Chem. Phys.* **2022**, *24* (42), 26200−26210.
(46) Vishwakarma, G.; Ghosh, J.; Pradeep, T. Desorption-Induced Evolution of Cubic and Hexagonal Ices in an Ultrahigh Vacuum and Cryogenic Temperatures. *Phys. Chem. Chem. Phys.* **2021**, *23* (41), 24052−24060.
(47) Watanabe, N.; Kouchi, A. Ice Surface Reactions: A Key to Chemical Evolution in Space. *Prog. Surf. Sci.* **2008**, *83* (10−12), 439−489.
(48) Ghosh, J.; Vishwakarma, G.; Das, S.; Pradeep, T. Facile Crystallization of Ice I_h via Formaldehyde Hydrate in Ultrahigh Vacuum under Cryogenic Conditions. *J. Phys. Chem. C* **2021**, *125* (8), 4532−4539.
(49) Avrami, M. Kinetics of Phase Change. II Transformation-Time Relations for Random Distribution of Nuclei. *J. Chem. Phys.* **1940**, *8*, 212−224.
(50) Harada, K.; Sugimoto, T.; Kato, F.; Watanabe, K.; Matsumoto, Y. Thickness Dependent Homogeneous Crystallization of Ultrathin Amorphous Solid Water Films. *Phys. Chem. Chem. Phys.* **2020**, *22* (4), 1963−1973.
(51) Hage, W.; Hallbrucker, A.; Mayer, E.; Johari, G. P. Crystallization Kinetics of Water below 150 K. *J. Chem. Phys.* **1994**, *100* (4), 2743−2747.
(52) Lee, D. H.; Kang, H. Acid-Promoted Crystallization of Amorphous Solid Water. *J. Phys. Chem. C* **2018**, *122* (42), 24164−24170.
(53) Avrami, M. Kinetics of Phase Change. II Transformation-Time Relations for Random Distribution of Nuclei. *J. Chem. Phys.* **1940**, *8* (2), 212−224.

https://doi.org/10.1021/acs.jpcc.3c07792
J. Phys. Chem. C 2024, 128, 2463−2470